EDGEWOOD

CHEMICAL BIOLOGICAL CENTER

U.S. ARMY RESEARCH, DEVELOPMENT AND ENGINEERING COMMAND

ECBC-TR-592

NMR IDENTIFICATION AND MS CONFORMATION OF THE SCOPOLAMINE NEUROTOXIN

Terry J. Henderson
Jonathan M. Oyler

RESEARCH AND TECHNOLOGY DIRECTORATE

David B. Cullinan

SCIENCE APPLICATIONS INTERNATIONAL CORPORATION
Abingdon, MD 21009

November 2007

Approved for public release;
distribution is unlimited.

ABERDEEN PROVING GROUND, MD 21010-5424

Disclaimer

The findings in this report are not to be construed as an official Department of the Army position unless so designated by other authorizing documents.

REPORT DOCUMENTATION PAGE

Form Approved
OMB No. 0704-0188

1. REPORT DATE *(DD-MM-YYYY)*	2. REPORT TYPE	3. DATES COVERED *(From - To)*
XX-11-2007	Final	Mar 2000 - Mar 2006

4. TITLE AND SUBTITLE

NMR Identification and MS Conformation of the Scopolamine Neurotoxin

5a. CONTRACT NUMBER

5b. GRANT NUMBER

5c. PROGRAM ELEMENT NUMBER

6. AUTHOR(S)

Henderson, Terry J.; Oyler, Jonathan M.(ECBC); and Cullinan, David B. (SAIC)

5d. PROJECT NUMBER
00P-0082

5e. TASK NUMBER

5f. WORK UNIT NUMBER

7. PERFORMING ORGANIZATION NAME(S) AND ADDRESS(ES)
DIR, ECBC, ATTN: AMSRD-ECB-RT-CF, APG, MD 21010-5424
SAIC, 3465A Box Hill Corporate Drive, Abingdon, MD 21009

8. PERFORMING ORGANIZATION REPORT NUMBER
ECBC-TR-592

9. SPONSORING / MONITORING AGENCY NAME(S) AND ADDRESS(ES)

10. SPONSOR/MONITOR'S ACRONYM(S)

11. SPONSOR/MONITOR'S REPORT NUMBER(S)

12. DISTRIBUTION / AVAILABILITY STATEMENT

Approved for public release; distribution is unlimited.

13. SUPPLEMENTARY NOTES

14. ABSTRACT

An unidentified white powder collected as evidence in an intelligence investigation was characterized exclusively by NMR analysis. A small fraction of the powder dissolved in D_2O was subjected to quantitative ^1H and $^{13}C\{^1H\}$ experiments and a series of two-dimensional correlation techniques, including ^1H-^1H COSY and NOESY as well as ^1H-^{13}C HSQC and HMBC spectroscopy. These were used to elucidate the molecular structure of the powder's major component and positively identify it as the scopolamine biotoxin. To confirm the NMR results, an ethanol/H_2O solution of the powder was analyzed by direct infusion into an ion trap mass spectrometer. A prominent base signal at m/z 304.1 was observed, consistent with the protonated molecular ion of scopolamine. Comparisons of ^1H and ^{13}C chemical shift values and J_{HH} values measured from the NMR data were found to agree very favorably with previously reported values for scopolamine in D_2O.

15. SUBJECT TERMS

Forensics	Molecular structure	Biological toxins	Tropane alkaloids
Nuclear magnetic resonance	Quantitation	Mass spectrometry	

16. SECURITY CLASSIFICATION OF:			17. LIMITATION OF ABSTRACT	18. NUMBER OF PAGES	19a. NAME OF RESPONSIBLE PERSON
					Sandra J. Johnson
a. REPORT	b. ABSTRACT	c. THIS PAGE			19b. TELEPHONE NUMBER *(include area code)*
U	U	U	UL	31	(410) 436-2914

Blank

PREFACE

The work described in this report was authorized under Project No. 00P-0082. The work started in March 2000 and was completed in March 2006.

The use of either trade or manufacturers' names in this report does not constitute an official endorsement of any commercial products. This report may not be cited for purposes of advertisement.

This report has been approved for public release. Registered users should request additional copies from the Defense Technical Information Center; unregistered users should direct such requests to the National Technical Information Service.

Acknowledgment

The authors would like to acknowledge Richard J. Lawrence, U.S. Army Medical Research Institute of Chemical Defense, Aberdeen Proving Ground, MD, for his invaluable mass spectrometry expertise.

Blank

CONTENTS

FIGURES

TABLES

NMR IDENTIFICATION AND MS CONFORMATION OF THE SCOPOLAMINE NEUROTOXIN

1. INTRODUCTION

As demonstrated by the recent attacks involving ricin (1, 2), biochemical weapons pose a threat not only to U. S. and Allied militaries but innocent civilians as well. The weapons are attractive to foreign states or terrorists seeking a mass-destruction capability, simply because they are relatively inexpensive to produce and do not require the elaborate technical infrastructure needed for nuclear weapons manufacturing. Biological toxins are poisonous compounds produced by different types of living organisms. Those that are highly toxic to humans and are stable, easily available and manageable are important for the threat they present. Chemically, the toxins are peptides or proteins of various sizes, large glycoproteins, polysaccharides, or other organic compounds of different sizes and structures. Bacterial toxins are proteins that are a normal part of the metabolic machinery of the pathogen. Algal toxins are produced by many different algae, and constitute a very diverse group of compounds ranging from simple ammonia to complex polypeptides and polysaccharides. Dynoflagellates are a source of some potent, nonprotein toxins such as saxitoxin and tetrodotoxin; one such toxin is the cause of red tide. Mycotoxins comprise a wide variety of nonprotein chemical substances produced by molds and fungi. Specific parts of some plants contain toxins which are extremely poisonous. The glycoproteins ricin from castor beans and abrin from Abrus seeds are examples of these plant toxins. Finally, there are a number of toxins produced by animals, including the nonprotein batrachotoxin from the Columbian frog, and a variety of peptide and proteins from marine snails, scorpion venoms and snake venoms.

Crimes and criminal actions involving biological toxins are explicitly described in Chapter 10 of Title 18 of the United States Code. In general, with the exception of certain representatives of the Federal Government, it is unlawful for anyone to develop, produce, acquire, stockpile, own, possess, use or threaten to use any biological toxin. This applies to all persons within the United States and U. S. Nationals in foreign countries. In addition, it is unlawful to use the toxins against a U. S. National outside of the United States, or while on any property that is owned, leased, or used by the United States or its Government, whether within or outside of the United States. Chapter 113B of the Title describes biological toxins as weapons of mass destruction, and the use of such weapons as acts of terrorism. Due to the September 2001 terrorist attacks in New York City and Washington, D. C., Chapters 10 and 113B were recently amended in House Resolution 3162, better known as the USA Patriot Act of 2001 (3). Many biological toxins are on the U.S. Munitions Import List defined in Title 27, Part 47 of the U. S. Code of Federal Regulations (27 CFR 47), and, therefore, their importation into the United States is unlawful for all individuals except those registered by the Director of the Department of Alcohol, Tobacco and Firearms.

Evidence from the scene of a terrorist or military attack suspected to involve a biotoxin weapon is usually taken to a forensic laboratory licensed to handle chemical

warfare agents and biochemical weapons. The single, most important determination that the laboratory must make is whether the sample contains toxic substances, particularly in the form of the weapons themselves, their degradation products, or impurities from their preparation. This information is important not only for legal evidence, but determines the sample's potential to harm laboratory personnel, and how the sample is to be handled during analysis. The strongest evidence for the presence of any toxic compound is its detection by chemical analysis together with a complete elucidation and conformation of its molecular structure. In the simplest cases, investigating officials have an idea of the chemical or biochemical weapon used from evidence collected at the scene of the attack, and the list of potential target analytes is small. Routine analytical techniques such as gas chromatography/mass spectrometry can be used to identify the weapon and verify its molecular structure. Evidence for the use of chemical or biotoxin weapons, however, is not always available. For example, the use of a biological weapon may only be surmised from symptoms exhibited by people at the scene of the attack, and the use of toxic industrial chemicals or other toxic materials cannot be ruled out. The list of potential target analytes and analytical methods required to evaluate samples, therefore, can grow very large. To complicate matters, after determining that a sample does not contain toxic or hazardous materials, criminal investigators may decide to characterize its chemical composition completely, further increasing the size of the potential target analyte list. In these cases, forensics laboratories turn to spectrometric techniques, like nuclear magnetic resonance (NMR) spectroscopy, to elucidate the molecular structure of the chemical components. Although more expensive and less sensitive than conventional techniques, NMR spectroscopy does not require extensive sample preparation, and generates results that are easily interpreted.

A complete structural determination was performed in an effort to characterize a forensic sample. Approximately 50 g of a white powder seized in an intelligence investigation were brought to the Forensic Analytical Team for chemical weapons screening. After testing negative for the suspected chemical weapons and their degradation products, the sample was analyzed further to identify its chemical composition. Relying heavily on two-dimensional NMR spectroscopy, the analysis positively identified the powder as the biological toxin scopolamine, a powerful antagonist of acetylcholine which is known to act at the autonomic parasympathetic post-ganglionic junction. Direct infusion positive electrospray ionization ion trap mass spectrometry (ESI^+-MS) was used as a complementary technique to confirm the NMR results. The details of this characterization and structural elucidation are presented herein.

2. EXPERIMENTAL PROTOCOLS

2.1 Chemicals, Solvents and Supplies

D_2O and $CDCl_3$ (both at ≥99% isotope enrichment), as well as the chemical shift reference compounds tetramethylsilane and the sodium salt of 3-(trimethylsilyl)-1-propane-sulfonic acid, were purchased from Sigma-Aldrich (St. Louis, MO). HPLC grade

ethanol and H_2O, and (-)-scopolamine hydrochloride were also purchased from Sigma-Aldrich. All NMR sample tubes were purchased from Wilmad-Labglass (Buena, NJ).

2.2 Sample Preparation

Samples were prepared as concentrated solutions in deuterated solvents for NMR spectroscopy. Approximately 56 mg of an unidentified white powder were dissolved into 1.25 mL D_2O, and determined to have a pD of 6.0 as described (4). A second solution was prepared in $CDCl_3$ at a concentration of ~20 mg/mL. Samples were placed into separate 5-mm NMR sample tubes just prior to NMR analysis. For mass spectrometric analyses, 1 mg of the powder was dissolved in 1 mL of 50% ethanol/50% H_2O (v/v) to give a 1 mg/mL stock solution. A 1:10 dilution of this stock with the same ethanol/H_2O solution was analyzed directly by ESI^+-MS and ESI^+-MS/MS.

2.3 NMR Spectroscopy

All NMR spectroscopy was conducted at 11.75 Tesla, using an Avance DRX-500 spectrometer (Bruker-Biospin Corp., Billerica, MA) with XWIN-NMR software (version 3.1) for data acquisition and processing. The spectrometer was fitted with a triple resonance TXI probe head (Bruker-Biospin Corp.) having dedicated ^1H, ^{13}C and ^{31}P channels (inverse-detection configuration) and actively shielded *x*-, *y*- and *z*-gradient coils. A three-channel, 10-ampere Acustar II 3x10 gradient amplifier (Bruker-Biospin Corp.) was used to amplify gradient coil pulses, with all pulse timing controlled from the spectrometer pulse programs. Experiments were conducted at 25.0±0.2 °C unless noted otherwise, with the sample spinning at 20 Hz for of one-dimensional experiments only. For two-dimensional spectroscopy, quadrature detection was used exclusively for collecting complex data in the direct dimension (t_2), while various phase cycling schemes used for the indirect dimension (t_1) gave either real or complex data. ^1H and ^{13}C chemical shifts were referenced to internal tetramethylsilane, or 3-(trimethylsilyl)-1-propane-sulfonic acid in the case of aqueous solutions.

2.3.1 Quantitative NMR Spectroscopy

All one-dimensional spectroscopy was conducted under quantitative conditions to determine the exact number of nuclei represented for each signal, imposing the need to evaluate spin-lattice relaxation time (T_1) values for all signals in the spectra. For both ^1H and ^{13}C spectroscopy, T_1 values were estimated from signal intensities in data sets using the inversion recovery pulse sequence [180°-τ-90°-acquisition] and a single exponential expression for T_1 (5). ^1H data sets were recorded with relaxation delays $\geq 5T_1$ for all signals, ensuring quantitative recovery between successive pulses. ^{13}C data sets derived from experiments using relaxation delays $\geq 8T_1$ (~20 s) to ensure the complete elimination of nuclear Overhauser effect (NOE) enhancements (6). Signal intensities were determined by electronic integration of expanded regions around the signals. Spectral regions chosen for integration included all spinning sideband and ^{13}C satellite signals originating from the parent signal.

^{1}H free induction decay data containing 16,384 or 65,536 complex points were recorded from the summation of 32 acquisitions using 10-12 ppm spectral windows, 90° pulse widths of 8.5 μs, and relaxation delays between 5-9 s. These data were Fourier transformed directly into spectra and manually adjusted into pure absorption mode.

All ^{13}C{^{1}H} data sets were recorded with 65,536 complex points, using 90° pulse widths of 11.3 μs, 220 ppm spectral windows, 20 s relaxation delays and inverse-gated ^{1}H decoupling (decoupling during data acquisition only) with a low-power, composite pulse sequence (7). Alternatively, quantitative ^{13}C{^{1}H} DEPT data sets were recorded using the sensitivity-enhanced Q-DEPT pulse sequence (8). Recorded data sets were multiplied by an exponential window function (apodized) with a line-broadening factor of 2 Hz before Fourier transformation into spectra and manual phase correction into pure absorption mode.

2.3.2 ^{1}H-^{1}H Correlation Spectroscopy

J-coupled ^{1}H pairs were identified with a pulsed-field gradient, double-quantum filtered, correlation spectroscopy (COSY) pulse sequence using a time proportional phase incrementation (TPPI) phase cycling (9) for quadrature detection in the indirect dimension. The data set contained 4096 free induction decays, each with 8192 complex points from two data accumulations using 1 s relaxation delays to give a final 4096 real X 8192 complex (t_1 X t_2) data matrix. Spectral windows of 6.4 ppm were used in both dimensions. The t_2 free induction decay data were zero-filled to 16,384 complex points, then apodized with a line-broadening factor of 0.5 Hz before Fourier transformation. The resulting t_1 free induction decay data were zero-filled to 8192 real points, apodized with a 1.5 Hz line-broadening factor, and finally Fourier transformed into a spectrum of 8192 X 8192 (f_1 X f_2) real points.

Dipolar-coupled ^{1}H pairs were found with a nuclear Overhauser effect spectroscopy (NOESY) (10) sequence incorporating gradient pulses during the mixing time (11) and a States-TPPI scheme to achieve quadrature detection in the indirect dimension (12). Data sets were recorded as a 512 X 2048 complex matrix using 6.6 ppm spectral windows in both dimensions. Each t_2 free induction decay resulted from eight data acquisitions with 4 s relaxation delays and 700 ms mixing times. The t_2 data were multiplied by a sine window function before Fourier transformation. The resulting t_1 data were extended to 2048 complex points with a linear prediction algorithm (13-15), multiplied by a sine window function, and finally Fourier transformed into a spectrum containing 1024 real data points in both dimensions.

2.3.3 ^{1}H-^{13}C Correlation Spectroscopy

One-bond ^{1}H-^{13}C correlations were determined with a heteronuclear, single quantum coherence (HSQC) pulse sequence using a pulsed-field gradient echo/antiecho-TPPI gradient scheme (16-18). A 1024 X 8192 complex data matrix was collected with six ^{1}H acquisitions per t_1 increment using 2 s relaxation delays. The spectral widths were 6.4 and 220 ppm in the ^{1}H and ^{13}C dimensions, respectively. ^{1}H data were apodized with a

4 Hz line-broadening factor before Fourier transformation. For t_1, data points were extended to 4096 complex points by linear prediction before multiplication with a sine-squared window function and final Fourier transformation into a 2048 X 4096 real spectrum.

Long-range, ^{1}H-^{13}C correlations were identified with a heteronuclear multiple bond correlation (HMBC) pulse sequence incorporating pulsed-field gradients for phase coherence selection and a low-pass *J*-filter to suppress one-bond correlations (19). Data were collected as a 512 real X 8192 complex matrix from 32 ^{1}H acquisitions per t_1 increment, each using 2 s relaxation delays. The spectral windows were identical to those in the HSQC experiment. ^{1}H data were multiplied by a trapezoidal window function before Fourier transformation to increase spectral resolution. ^{13}C data were extended to 1024 real points by linear prediction before multiplication by a sine squared window function and Fourier transformation into a 1024 X 4096 real spectrum.

2.3.4 Diffusion Oriented Spectroscopy

Data sets for diffusion ordered spectroscopy (DOSY) spectra were acquired with the longitudinal eddy current delay pulse sequence of Gibbs and Johnson (20), which incorporates a delay at the end of the experiment for avoiding spectral artifacts from residual eddy currents. For the spectrometer and probe head, the optimum value of the eddy current delay was found to be 5.0 ms. In addition, a presaturation pulse was incorporated into the pulse program to attenuate the solvent signal and increase analyte sensitivity. The experiments also incorporated 50 ms diffusion time delays and either 1.2 or 1.5 ms gradient pulses for recording data sets at 25 or 37 °C, respectively. ^{1}H data sets acquired with 10 ppm spectral windows, 90° pulse widths and 6 s relaxation delays were recorded onto computer disk. The recorded data sets were multiplied by an exponential window function with a line-broadening factor of 1 Hz before Fourier transformation into spectra and manual adjustment into pure absorption mode. For each diffusion measurement, spectra from 16 separate data sets were collected as a function of gradient amplitude ranging between 2-95%.

2.4 Mass Spectrometry

Following NMR characterization, ESI^{+}-MS was performed on the sample with a Finnigan LCQ DECA ion-trap mass spectrometer (Thermoquest/Finnigan Corp., San Jose, CA), using a spray potential of 5 kV and a constant capillary temperature of 250 °C. The 0.1 mg/mL sample solution was directly infused for approximately 1 m at 3 μL/m, and averaged spectra were collected. Initially, spectra were collected in full scan mode (mass range 35-1000 amu), and a prominent base peak at m/z 304.1 was observed. Subsequently, the mass spectrometer was operated in zoom scan centered on 300±50 amu to identify the scopolamine molecular ion $(M+H)^{+}$. In product-ion scan mode, the m/z 304.1 ion was collected and subjected to 26% relative collision energy using nitrogen as a collision gas. Collision-induced dissociation (CID) produced major fragment ions at m/z 138.1 and 156.1.

3. RESULTS AND DISCUSSION

3.1 NMR Identification and ESI^+-MS Conformation of Scopolamine

An unidentified white powder seized in an intelligence investigation was brought to the Forensic Analytical Team for detailed chemical analysis. Preliminary tests found that the powder did not contain chemical warfare agents (particularly the nerve agent VX or sulfur mustard blister agents) or their degradation products as initially suspected. The powder was then subjected to an extensive NMR analysis to characterize its principal components. A flowchart illustrating the order in which the NMR experiments were performed, and the conclusions deriving from them, is presented in Figure 1.

Solubility tests at room temperature found that the powder was freely soluble in H_2O, $CHCl_3$, ethanol and acetone, and because the H_2O signal did not appear to obscure ^1H analyte signals, the powder was dissolved directly into D_2O for NMR analysis. A quantitative $^{13}C\{^1H\}$ spectrum of this sample is presented in Figure 2, where the signals are lettered in order of decreasing chemical shift, and a quantitative ^1H spectrum is shown in Figure 3. Carbon atoms were correlated to their directly bonded protons using the HSQC spectrum in Figure 4, and the information has been appended onto Figure 3.

The quantitative spectra were examined first to determine the exact number of compounds comprising the powder and as much information relating to their structural formulas as possible. Integration of the ^1H signals revealed 20 unique ^1H sites in addition to that for the solvent. DOSY analysis revealed that all analyte protons had identical diffusion rates at 25 and 37 °C (not shown), demonstrating conclusively that they all reside on the same molecule. The ^{13}C spectrum revealed 17 novel carbon atom sites, with 15 representing carbon atoms directly bonded to protons identified in the ^1H spectrum (see Figure 4). It was assumed that the remaining two ^{13}C signals also represented carbon atoms of the same molecule, since their measured integral values were virtually identical to those of many of the other carbon atoms. Signals were not detected with conventional ^{19}F and ^{31}P analyses, and ^{14}N spectroscopy revealed a single signal at 373 ppm (not shown). Finally, a quantitative ^1H spectrum of the powder dissolved in $CDCl_3$ contained an additional signal at 12.7 ppm (not shown), most likely from a single hydroxyl group

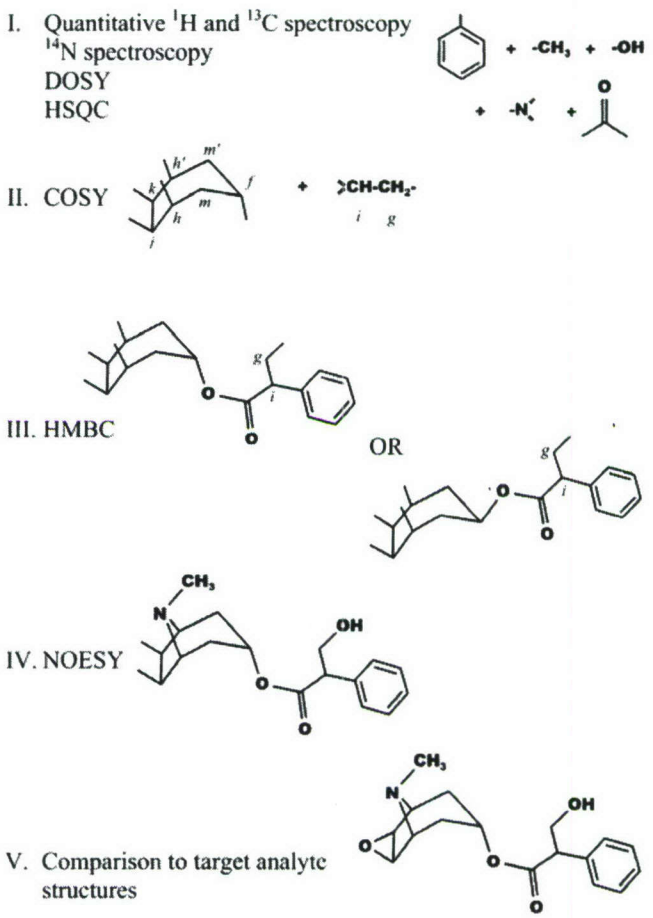

Figure 1. Summary of Experiments Used to Analyze the Unidentified Powder Dissolved in D_2O and the Structural Information Derived from Each. Italicized letters designating individual carbon sites derive from Figure 2, with primed (') and unprimed pairs of letters representing different sites on the ring system correlating to the same ^{13}C signal. Tropane ring positions are numbered in the bottom panel.

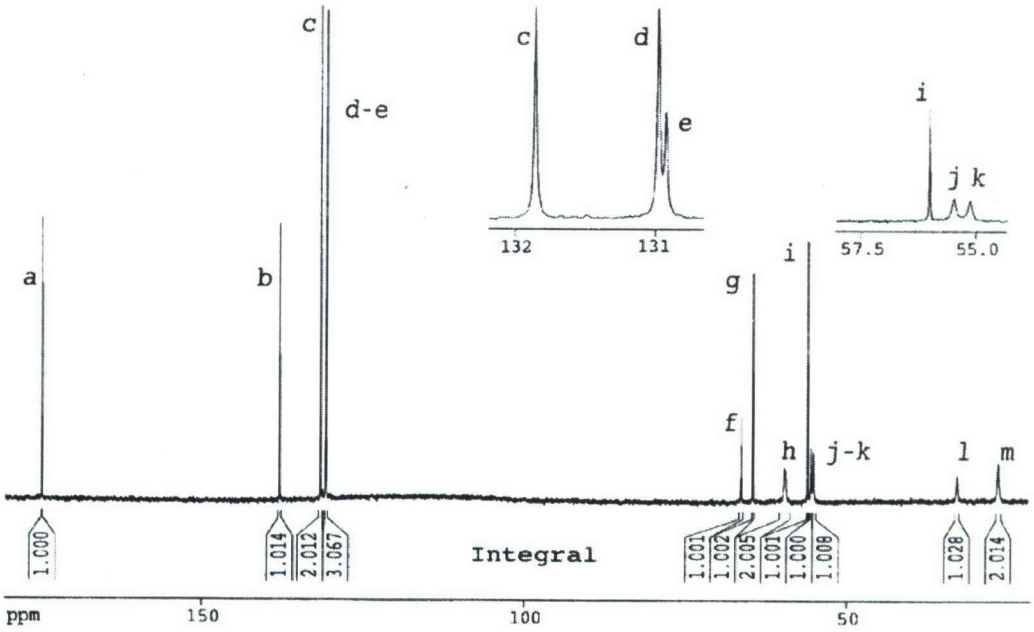

Figure 2. $^{13}C\{^{1}H\}$ Spectrum of the Unidentified Powder Dissolved in D_2O Acquired under Quantitative Conditions. Signals are lettered in order of increasing chemical shift (increasing resonance frequency), and their relative integral values are included. Insets show details of overlapping signals.

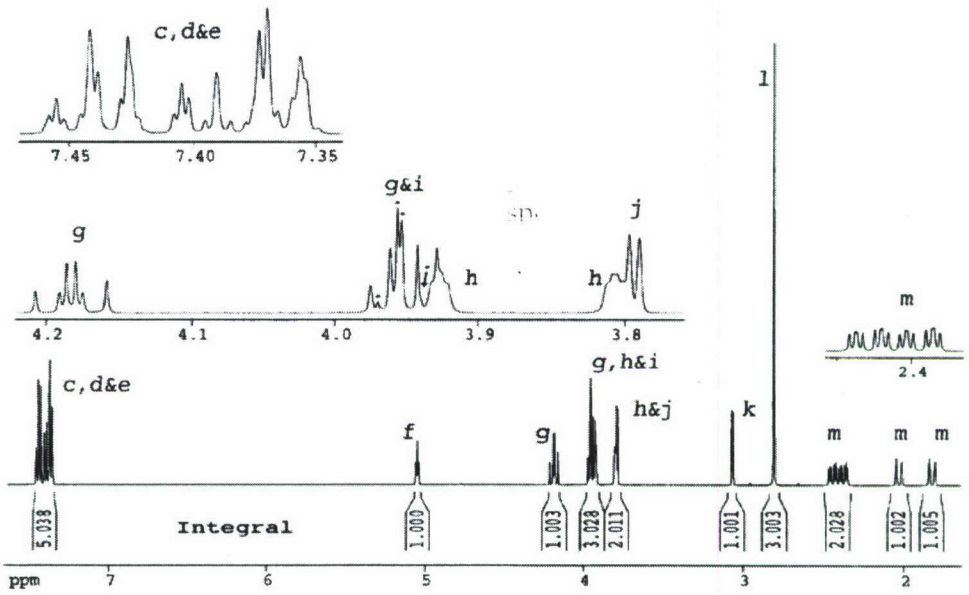

Figure 3. Quantitative ^{1}H Spectrum of the Unidentified Powder Dissolved in D_2O with Relative Integral Values Shown for All Signals. Letters assigned to signals relate their protons to the signal for their directly bonded carbon atom (Figure 2), determined from HSQC spectroscopy (Figure 4). Insets reveal details of complex spectral figures, with solid circles designating individual resonances for signal *i*.

The number of protons directly bonded to each carbon atom was determined by evaluating the quantitative spectra together with the HSQC correlations, leading to the identification of additional structural features. Four signals in the aromatic region of the ^{13}C spectrum (*b*, *c*, *d* and *e* in Figure 2) arise from six carbon atoms, and, therefore, are indicative of a single benzyl group. This conclusion is corroborated by the HSQC data, which correlates three of these signals to others occurring within the aromatic region of the ^{1}H spectrum (*c, d & e* in Figures 3 and 4). The ^{1}H spectrum illustrates further that these signals represent five protons, all of which appear to be intimately *J*-coupled to one another. In another region of the ^{13}C spectrum, a single carbon atom appears to be bound directly to three, magnetically equivalent protons (*l* in Figure 4), clearly representing a single methyl group.

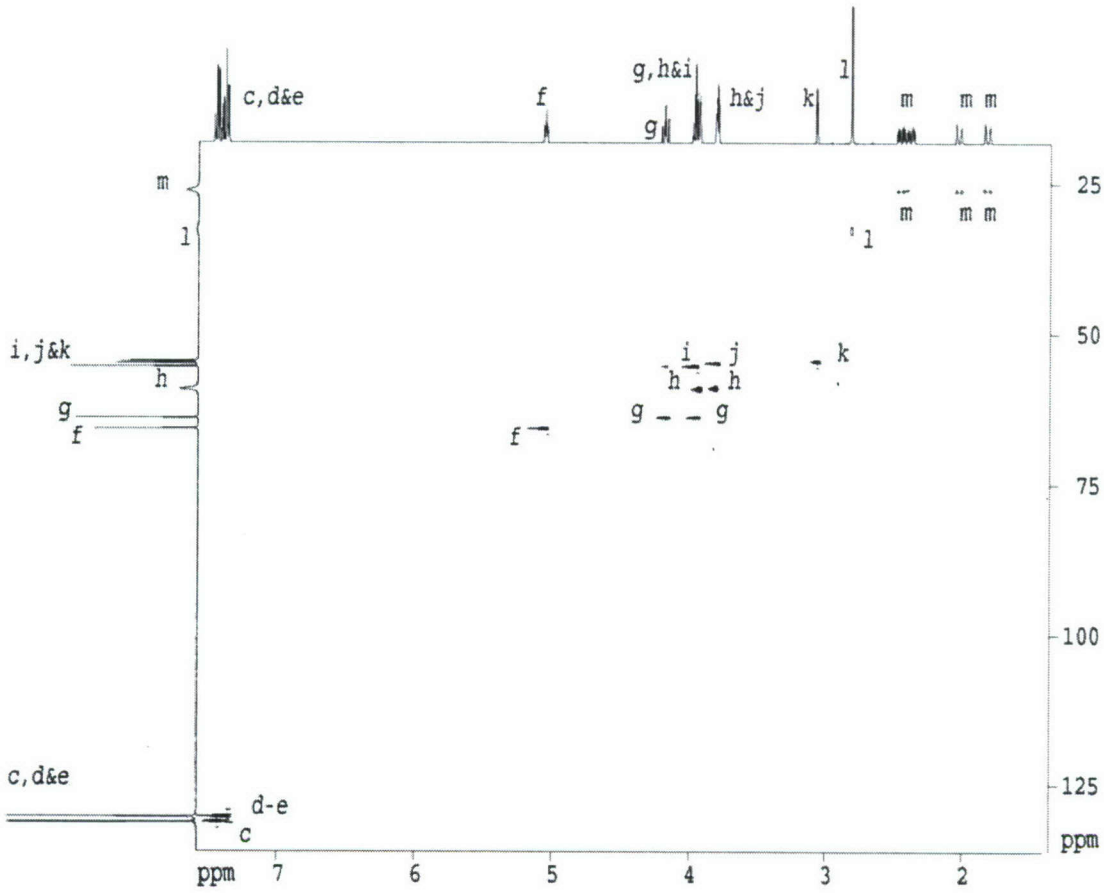

Figure 4. ^{1}H-^{13}C HSQC Spectrum of the Unidentified Powder Dissolved in D_2O, with the Corresponding One-Dimensional Sub-Spectra Included for Both Dimensions. The lettering scheme is from Figure 2.

The remaining structural features were inferred from $J_{H,H}$ networks revealed by the COSY spectrum in Figure 5. Two completely isolated coupling networks are apparent in addition to that of the benzyl group: a three-proton network (*g-g* & *g-i*), and a much more extensive nine-proton network. Careful examination of the correlations demonstrates that the latter arises from a ring system of seven carbon atoms (see the arrows in Figure 5). Starting with the autocorrelation for proton *f* (*f-f*), three correlations (*f-m*, *m-h* and *h-j*) define an unbranched, aliphatic chain of four carbon atoms. Another set of correlations (*f-m'*, *m'-h'* and *h'-k*) reveals a similar chain also starting with proton *f*, and a final correlation (*j-k*) connects the ends of these chains to close the ring. Strong coupling is evident between four of the ring system protons (δ_H=1.75-2.55 ppm), all of which are correlated to the same ^{13}C signal by HSQC spectroscopy (*m* in Figure 4). It is apparent that these protons are the axial-equatorial pairs for carbon atoms *m* and *m'* on the ring (see Figure 1). In the case of cyclohexane rings, equatorial proton signals are consistently found downfield (higher δ_H value) from those of the axial protons bonded to the same carbon atom (21), and signals were assigned to the protons accordingly (see Figure 7 for

assignments). In the three-proton network, the protons all correlate to one of two carbon atoms (*i* and *g* in Figure 4, referred to as C*i* and C*g*, respectively), clearly the consequence of a $-CH_2$ and CH group directly bonded to one another. Moreover, because C*i* and C*g* chemical shifts are far from the alkene region (δ_C=80-160 ppm), this bond must be a single, rather than a double bond (see Figure 1).

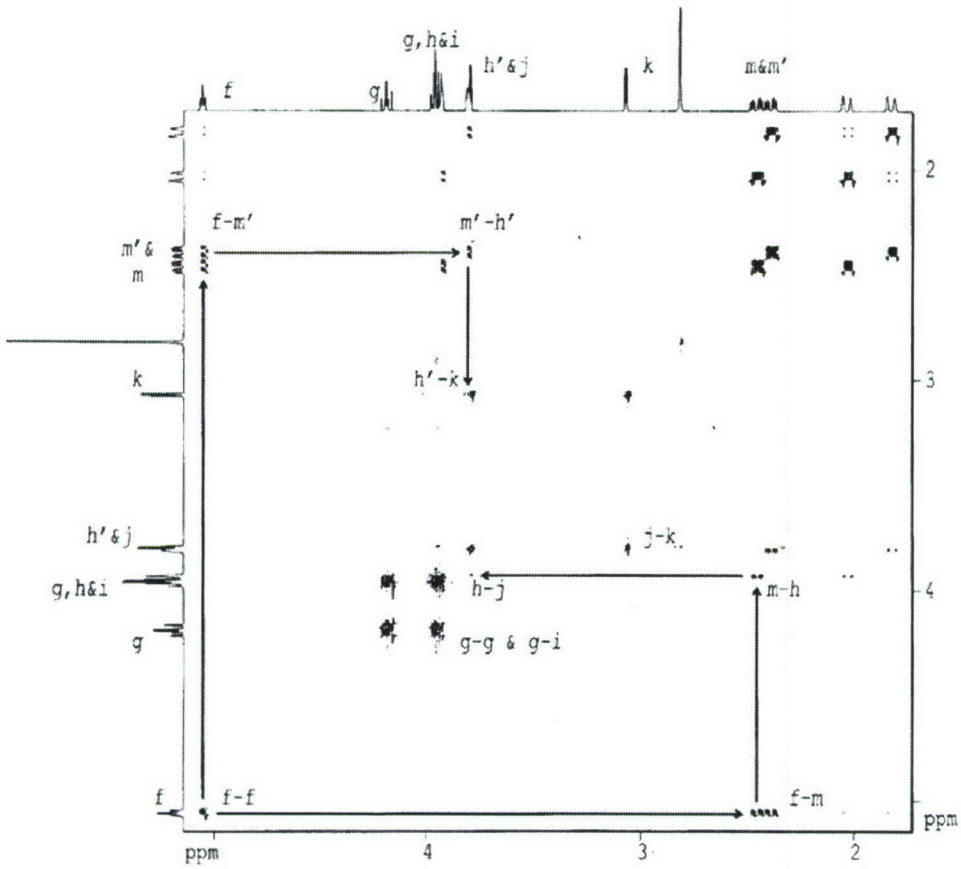

Figure 5. COSY Sub-Spectrum of the Unidentified Powder Dissolved in D_2O with the Corresponding Region of the ^1H Spectrum Shown for Both Dimensions. Correlations from a three-proton (*g-g & g-i*) and a nine-proton (*f-m*, *m-h*, *h-j*, *f-m'*, *m'-h'*, *h'-k* and *j-k*) $J_{H,H}$ network are designated. Arrows illustrate the $J_{H,H}$ connectivity for the latter network, defining a seven carbon atom ring system. All lettering is consistent with Figures 1 and 3.

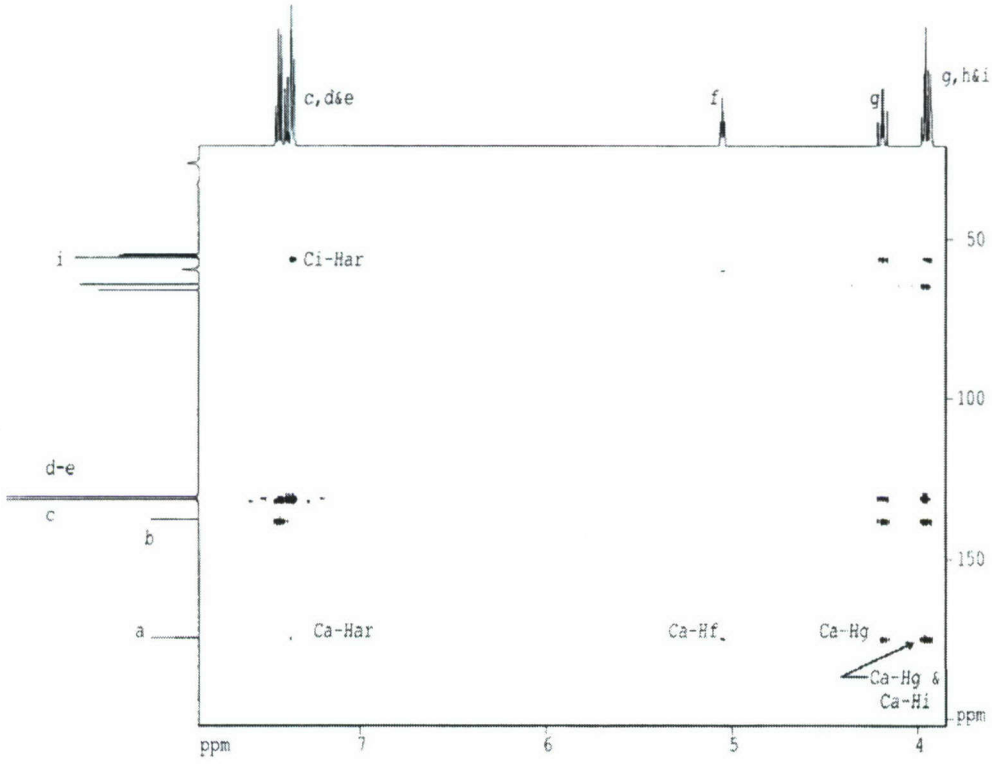

Figure 6. ^{1}H-^{13}C HMBC Sub-Spectrum of the Unidentified Powder Dissolved in D_2O with the Corresponding Regions of the ^{1}H and $^{13}C\{^{1}H\}$ Spectra. Long-range correlations demonstrating the connectivities of specific chemical groups in the molecule are labeled.

Long-range ^{1}H-^{13}C correlations were identified by HMBC spectroscopy and were used to assemble the identified structural elements into a molecular structure. The experiment incorporates a specific delay for the evolution of long-range scalar couplings, and the detected correlations are a direct function of the delay. In the particular case of hydrocarbons, a relationship between $^{3}J_{CH}$ values and H-C-C dihedral angles has been suggested (22) which can be used to derive a delay time. A region of the HMBC spectrum displaying all relevant correlations is shown in Figure 6. Long-range correlations were found between the aromatic protons H*ar* and the carbonyl carbon atom (C*a*-H*ar*), as well as carbon atom C*i* (C*i*-H*ar*). The substantially larger intensity of C*i*-H*ar* suggests that the benzyl group is directly bonded to C*i*, however, the detection of C*a*-H*ar* demonstrates that C*a* must also be in close proximity to the benzyl group. In addition to C*a*-H*ar*, four other C*a* correlations to remote protons are observed: C*a*-H*f*, two C*a*-H*g* correlations, and C*a*-H*i*. These can be rationalized by placing the carbonyl carbon atom between C*f* on the ring system and the CH_2CH moiety. A single bond was assigned between C*a* and C*i* because its corresponding correlation is significantly more intense than all other C*a* correlations with remote protons. Furthermore, the C*a*-H*ar* correlation is more likely a consequence of this bond rather than one between C*a* and C*g*, since the latter requires the unlikely detection of a five-bond correlation. For the connectivity between C*a* and C*f*, the much lower intensity of the C*a*-H*f* correlation relative the C*a*-H*i* and C*a*-H*g* intensities suggests that the two carbon atoms are not directly bonded, but that another atom occurs between them. An oxygen atom was tentatively assigned to be bound to both C*a* and C*f*, because

all ^{13}C signals have already been assigned to structural elements, and the chemical shifts of the H*f* and C*f* signals are more indicative of an oxygen atom at this site rather than a nitrogen atom. The absolute configuration about C*f* cannot be surmised from the COSY, HSQC, or HMBC data, and, therefore, both axial and equatorial C*f*-O bonds are possible (see Figure 1).

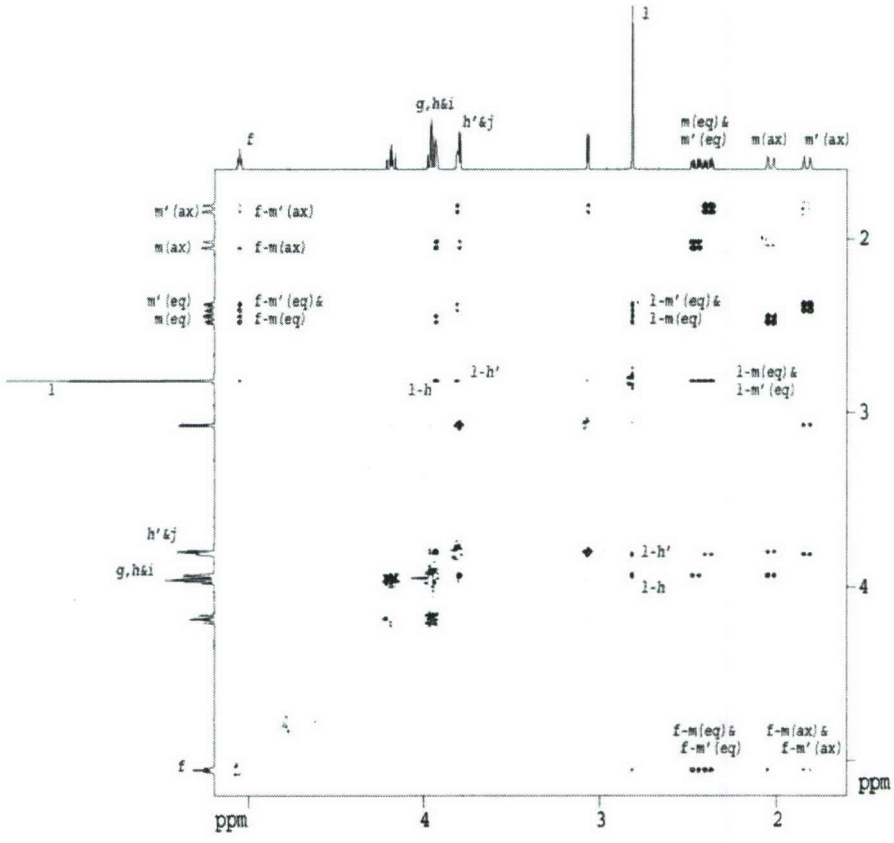

Figure 7. NOESY Sub-Spectrum of the Unidentified Powder Dissolved in D_2O with the Corresponding Region of the ^1H Spectrum Shown for Both Dimensions. Correlations placing the methyl group in conformational space, and the configuration about carbon atom *f*, are designated.

The final experimental effort relied on NOESY to place the nitrogen atom, the methyl group and the hydroxyl group within the conformational space around the two ring systems in order to infer their connectivities to specific atoms of the analyte molecule. The region of the NOESY spectrum illustrating key correlations is shown in Figure 7. For the methyl protons (H*l*), strong correlations with the protons of C*h*, C*h*', C*m* and C*m'* (labeled, respectively, as *l-h*, *l-h*', *l-m*(eq) and *l-m'*(eq)), all with very similar intensities, suggest that the methyl group occurs at a position equidistant from the four carbon atoms. Moreover, because the *l-m* and *l-m'* correlations involve the equatorial rather than axial protons, the methyl group must occur on the same side of the seven carbon atom ring system as the equatorial protons. The observations can be explained by connecting the nitrogen atom to both C*h* and C*h*', and in turn, connecting the methyl group directly to the nitrogen atom in a configuration holding the methyl group between and above C*m* and C*m*' (see Figure 1).

Other NOESY correlations can be used to determine the configuration about C*f*. The much more intense *f*-*m*(eq) and *f*-*m*'(eq) correlations relative to *f*-*m*(ax) and *f*-*m*'(ax) for example, demonstrate that the C*f*-H*f* bond occurs at the equatorial position, leaving the C*f*-O bond in the axial position and on the opposite side of the ring system from the methyl group. Finally, a NOESY spectrum of the compound dissolved in $CDCl_3$ (not shown) contained intense correlations between the hydroxyl group ^1H and both H*g* signals, implicating that the hydroxyl group is directly bonded to C*g*.

With the exception of the remaining connectivities for C*j* and C*k*, the structure has been completely elucidated. From the one-dimensional NMR data, it is clear that these connectivities do not involve carbon, nitrogen, phosphors or fluorine atoms, or other protons. Signals H*j* and H*k* display no evidence of *J*-coupling to NMR-active nuclei other than each other, eliminating any utility for further NMR spectroscopy. At this point, the molecular structures of target analytes were considered to provide clues, and it was discovered that by simply connecting C*j* and C*k* with a single oxygen atom to create an epoxy group (see Figure 1), a tropane ring system could be formed to generate the structure of the scopolamine neurotoxin ($C_{17}H_{21}NO_4$, 303.35 g/mole). ^1H and ^{13}C spectroscopy of authentic scopolamine dissolved in D_2O (not shown) validated the sample as scopolamine.

The NMR results were corroborated by ESI^+-MS and ESI^+-MS/MS of a 0.1 mg/mL solution of the unknown powder. As shown in Figure 8, a clean electrospray mass spectrum with a prominent base signal centered at m/z 304.1 was produced. Additional signals were observed at m/z 305.1 and 306.1, corresponding, respectively, to 19 and 3% of the m/z 304.1 ion intensity. Also evident is a low intensity m/z 325.9 signal consistent with the sodium adduct $(M+Na)^+$ of scopolamine. Increases in ionization potential produced corresponding relative increases in m/z 138.1 and 156.1 intensity, and MS/MS also produced major characteristic fragments at m/z 138.1 and 156.1; see Figure 9.

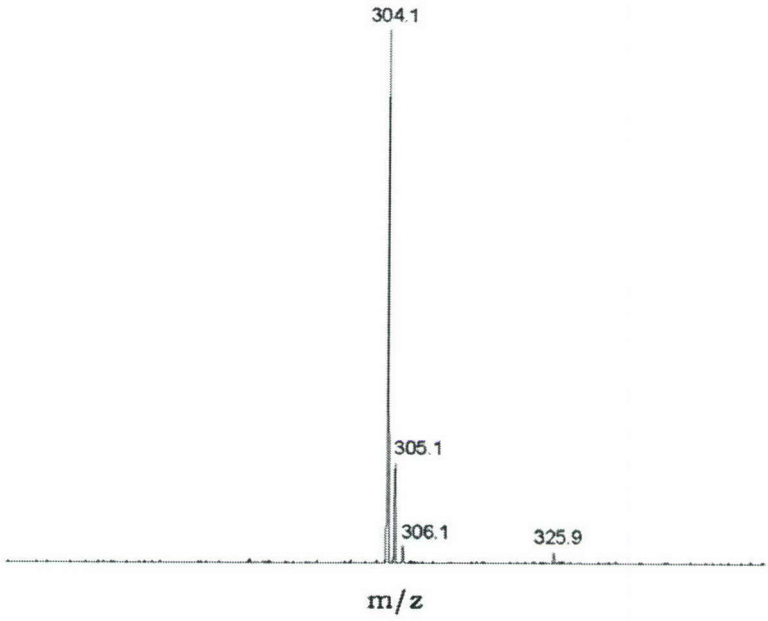

Figure 8. Mass Spectrum (250-350 Amu Zoom Scan) of the Unidentified White Powder Dissolved in 50% Ethanol/50% H_2O (*v/v*).

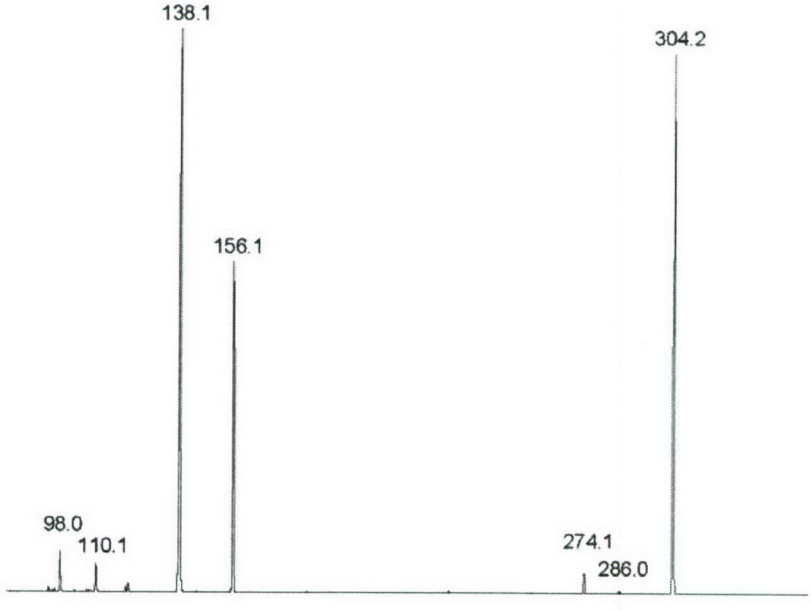

Figure 9. ESI+-MS/MS Spectrum of the Unidentified Powder Base Signal, m/z 304.1.

The prominent m/z 304.1 base signal (Figure 8) supports the molecular formula $C_{17}H_{21}NO_4$ for the powder's major component, and further, is consistent with the molecular ion $(M+H)^+$ of scopolamine. The isotope pattern observed agrees very favorably with the theoretical values for this formula (19 and 3% observed, compared to the calculated values of 19.7 and 2.6%, respectively). In-source fragmentation and MS/MS data support this conclusion as well, and both are consistent with previous reports (23-25). The m/z 156.1 major fragment can be attributed to cleavage of the bond between the carbonyl carbon and the ester oxygen on the tropane ring, with charge retained on the ring to leave a m/z 156 fragment. Likewise, the m/z 138 fragment corresponds to the m/z 156 fragment with a loss of water (23-25).

3.2 Comparison of NMR Results to Previously Reported Data

There are a significant number of NMR investigations in the literature addressing scopolamine structure (26-42) that permit direct comparisons between the measured NMR parameters in this study and previously published values. Several such comparisons have been made in this study for the chemical shift and $J_{H,H}$ measurements, and these comparisons are presented in table form. Table 1 summarizes comparisons of our ^1H and ^{13}C chemical shift measurements to previously reported values from three different reports, while Table 2 lists the $J_{H,H}$ measurements for the scopolamine tropane ring protons and those from an earlier report. In both tables, the tropane ring positions used to identify individual carbon atoms (C-1 to C-7) and protons (H-1 to H-7, including all axial, *ax*, and equatorial, *eq*, protons) are illustrated in the bottom panel of Figure 1.

The ^{13}C chemical shift measurements agree favorably with previously reported values for scopolamine in D_2O. Table 1 reveals that the ^{13}C chemical shift measurements for the scopolamine tropane ring from this stusy closely resemble those of Feeney and coworkers (32), who reported the first ^{13}C chemical shift measurements for the toxin in D_2O. Their assignment of 25.27 ppm for the *N*-methyl group signal, however, differs significantly with the finding of 32.72 ppm for the same signal in this study. This reflects the confusion observed in the earlier literature regarding the ^{13}C chemical shift of this group for the toxin in D_2O (38, 39). Glaser *et al.* (36) ultimately resolved this confusion by demonstrating that the *N*-methyl group stereochemistry of tropane alkaloids is strikingly solvent sensitive (see *ref.* 39 for a detailed discussion). The measured ^{13}C chemical shift for this group agrees well not only with that of Glaser *et al.*, but also with a later report from the same laboratory (42). Furthermore, all of the ^{13}C chemical shift measurements from this study are remarkably similar to their corresponding values from this latter report (42). Each set of measurements from this study differs by less than 0.15 ppm from their previously reported value, and most values differ by less than 0.10 ppm.

Table 1. ^{13}C and ^{1}H Chemical Shift Values (ppm) for Scopolamine in D_2O

^{13}C Chemical Shifts (δ)					^{1}H Chemical Shifts (δ)		
^{13}C Site	Current Data	Reference (32)	Reference (36)	Reference (42)	^{1}H Site	Current Data	Reference (32)
C=O	175.01	*	174.86	175.05	H(*meta*)	7.44	*
C(*ipso*)	138.12	*	138.16	138.28	H(*ortho*)	7.43	*
C(*meta*)	131.85	*	130.85†	131.93	H(*para*)	7.37	*
C(*ortho*)	130.98	*	131.66†	131.04	H-3	5.06	5.05
C(*para*)	130.93	*	130.69	130.99	$-CH_{2a}-$	4.19	*
C-3	66.31	64.68	66.05	66.26	-CH(*Ph*)-	3.97	*
$-CH_2-$	64.49	*	64.57	64.64	$-CH_{2b}-$	3.96	*
C-5	59.52	58.27	59.48	59.65	H-5	3.94	3.94
C-1	59.39	58.13	59.34	59.49	H-1	3.82	3.82
-CH(*Ph*)-	56.01	*	56.06	56.17	H-6	3.80	3.80
C-6	55.48	53.92	55.01	55.52	H-7	3.06	3.07
C-7	55.13	53.57	55.30	55.17	$N-CH_3$	2.82	*
$N-CH_3$	32.72	25.72	32.74	32.83	H-4*ax*	2.47	2.47
C-2	26.22	25.20	26.10‡	26.33	H-2*ax*	2.40	2.40
C-4	26.13	25.20	26.22‡	26.22	H-4*eq*	2.04	2.04
					H-2*eq*	1.82	1.82

* Not determined.
† Assignments reversed in *ref.* (36) and corrected in *ref.* (42)
‡ Assignments reversed in *ref.* (36) and corrected in *ref.* (42)

In contrast to ^{13}C chemical shift data, the literature contains very little information concerning ^{1}H chemical shift measurements for scopolamine in D_2O. Although Feeney and coworkers (32) do report such measurements, these are limited to only the tropane ring proton signals. In general terms, the ^{1}H chemical shift measurements from this study are identical, or essentially identical, to these earlier measurements. As shown more specifically in Table 1, seven of the measurements from this study are identical to their corresponding values appearing in the earlier report, and the remaining two differ from their previously reported values by only 0.01 ppm. The table also lists the ^{1}H chemical shift measurements from this study for the remaining scopolamine protons. Corresponding values for these protons are reported for scopolamine in CD_2Cl_2 (36) and $CDCl_3$ (35, 38); however, no comparisons were made of chemical shift values derived from different solvents, as solvent effects can significantly impact chemical shift values. The H-4*ax* signal for example, is found at 2.47 ppm from the measurements in this study (see Table 1) and others (32) for the toxin in D_2O, but appears at 3.31 and 2.08 ppm for the toxin in CD_2Cl_2 (36) and $CDCl_3$ (38), respectively. Such differences can appear discordant without detailed explanations, and offer little when attempting to corroborate different sets of data.

As for the ^{1}H chemical shift data, Feeney and coworkers (32) report the only $J_{H,H}$ measurements for scopolamine in D_2O, and these are again confined to only the tropane ring protons. These measurements and those from this study are listed in Table 2 for direct comparison. In general, the two sets of measurements are in good agreement with each

other. Of the nine pairs of corresponding values listed in the table, only two, $J_{1,2eq}$ and $J_{4eq,5}$, appear to possibly reflect minor disparities. It is not clear whether these differences result from measurement errors or differences in tropane ring conformation.

Table 2. Tropane Ring $J_{H,H}$ (Hz) Values for Scopolamine in D_2O

$J_{H,H}$	Current Data	Reference (32)
$J_{1,2ax}$	1.4	1.3
$J_{1,2eq}$	3.5	4.8
$J_{2ax,2eq}$	17.3	17.3
$J_{2ax,3}$	5.0	3.8 *
$J_{2eq,3}$	1.0	1.0 *
$J_{1,7}$	0.7	<2.0
$J_{4eq,5}$	3.5	4.8
$J_{5,6}$	1.8	<2.0
$J_{6,7}$	3.5	3.6

* Measurements reversed in *ref.* (32) and corrected in *ref.* (36)

Finally, Sarazin *et al.* (38) report results from a ^1H-^1H chemical shift correlation and a long-range, ^1H-^{13}C chemical shift correlation for scopolamine in $CDCl_3$, experiments which are analogous to the COSY (Figure 5) and HMBC (Figure 6) experiments of this study. In large part, spectra from this study resemble those from the earlier report, even though they were conducted with the toxin in D_2O. Most importantly, all correlations identified by these experiments appear to have a corresponding correlation in the earlier reported spectra. Some significant differences are apparent, on the other hand, which give the spectra in this study somewhat of a different appearance. The most striking difference is that these spectra have considerably more resolution, a consequence of the use of a higher magnetic field strength (the earlier data were recorded at 7.06 Tesla), and in the case of the COSY experiment in this study, the use of phase sensitive pulse sequences rather than those sequences generating magnitude spectra. Another major source leading to spectral differences is the disparity in chemical shift values of the scopolamine protons for the two solvents. This is particularly the case for H-1, H-5 and H-6, which appear between 3.80-3.94 ppm in D_2O (see Table 1), but between 2.94-3.37 ppm in $CDCl_3$, placing correlations for these protons in different regions of the COSY and HMBC spectra from this study relative to their respective, previously published spectra. Although comparisons to chemical shift correlation spectra for scopolamine in D_2O would have been more appropriate, no such spectra appear in the literature.

4. CONCLUSIONS

Several NMR techniques were used in this study to characterize an unidentified white powder seized in an intelligence investigation. Collectively, the techniques were able to give a good estimate of the specific types and number of different atoms comprising the principal component of the powder, and essentially all of the information necessary to determine its chemical structure. This structure was easily elucidated, positively identifying the principal component as scopolamine. This investigation is just one example of an ever increasing number of forensic investigations involving biotoxins in crimes and acts of terror. In recent years, technical information relating to biochemical weapons has become readily accessible on the internet, and today, many of the materials for their isolation and purification are available for legitimate commercial purposes. The capability of hostile nations and terrorist groups for acquiring these weapons is greater now than at any other time in history. For these reasons, the analysis of law enforcement and intelligence samples for biological toxins has never been more important. Although more routine techniques relying on spectral libraries and other analytical data such as chromatographic retention times can be rapid and effective, they do not always lead to a positive identification of biological toxins. This is particularly the case for larger protein toxins such as ricin, staphylococcal enterotoxins and botulinum neurotoxins, where reliable detection can be a formidable challenge. Further, impurities that are valuable in determining which government, country or terrorist group has purified or supplied the weapon usually do not appear in spectral libraries. And there is an ever increasing likelihood of encountering unique toxins which are evolutionarily related to the more commonly known toxins (at least five evolutionarily related tetrodotoxins have been identified for example, see *refs.* 43 and 44), chemically modified nonprotein toxins, or even emerging threat agents such as genetically engineered protein toxins (45-50). In such cases, the elucidation of analyte molecular structure by interpretative means may present the best, and sometimes only, means for identification. While several techniques can provide valuable information for determining molecular structure, NMR spectroscopy remains one of the single most powerful techniques for providing detailed and unambiguous structural information within a reasonable timeframe. Moreover, the quantity and quality of structural data deriving from NMR experiments have been expanded considerably with the intense development of multi-dimensional techniques over the last 25 years, making NMR spectroscopy indispensable in forensic science today.

Blank

LITERATURE CITED

1. Eggen, D. Letter with Ricin Vial Sent to White House. *The Washington Post,* Feb 4, 2004, Sect. A7.

2. Fox, B. Ricin Found in Jars of Baby Food in California. *The Washington Post,* Jul 28, 2004, Sect. A6.

3. House Resolution 3162. *Uniting and Strengthening America by Providing Appropriate Tools Required to Intercept and Obstruct Terrorism* (USA PATRIOT ACT) Act of 2001. 107th Congress, 1st Session, Washington, DC, 24 October 2001.

4. Bates, R.G. *Determination of pH: Theory and Practice*; John Wiley and Sons, Inc.: New York, 1964; 219-20.

5. Farrar, T.C.; Becker, E.D. *Pulse and Fourier Transform NMR*; Academic Press: New York, 1967; 278-86.

6. Opella, S.J.; Nelson, D.J.; Jardetzky, O. ^{13}C Nuclear Magnetic Resonance Study of Molecular Motions and Conformational Transitions in Muscle Calcium Binding Parvalbumins. *J. Chem. Phys.* **1976**, *64*, 2533-5.

7. Shaka, A.J.; Keeler, J.; Freeman, R. Evaluation of a New Broadband Decoupling Sequence: WALTZ-16. *J. Magn. Reson.* **1983**, *53*, 313-40.

8. Henderson, T.J. Sensitivity-Enhanced Quantitative ^{13}C NMR Spectroscopy via Cancellation of $^{1}J_{CH}$ Dependence in DEPT Polarization Transfers. *J. Am. Chem. Soc.* **2004**, *126,* 3682-3.

9. Redfield, A.G.; Kunz, S.D. Quadrature Fourier NMR Detection: Simple Multiplex for Dual Detection and Discussion. *J. Magn. Reson.* **1975**, *19*, 250-4.

10. Jeener, J.; Meier, B.H.; Bachmann, P.; Ernst, R.R. Investigation of Exchange Processes by Two-Dimensional NMR Spectroscopy. *J. Chem. Phys.* **1979**, *7,* 4546-53.

11. Wagner, R.; Berger, S. Gradient-Selected NOESY - a Fourfold Reduction of the Measurement Time for the NOESY Experiment. *J. Magn. Reson. Series A* **1996**, *123*, 119-21.

12. States, D.J.; Haberkorn, R.A.; Ruben, D.J. A Two-Dimensional Nuclear Overhauser Experiment with Pure Absorption Phase in Four Quadrants. *J. Magn. Reson.* **1982**, *4,* 286-92.

13. Gesmar, H.; Led, J.J. Spectral Estimation of Two-Dimensional NMR Signals by Applying Linear Prediction to Both Dimensions. *J. Magn. Reson.* **1988**, *76*, 575-86.

14. Zeng, Y.; Tang, J.; Bush, C.A.; Norris, J.R. Enhanced Spectral Resolution in 2D NMR Signal Analysis Using Linear Prediction Extrapolation and Apodization. *J. Magn. Reson.* **1989**, *83*, 473-83.

15. Olejniczak, E.T.; Eaton, H.L. Extrapolation of Time-Domain Data with Linear Prediction Increases Resolution and Sensitivity. *J. Magn. Reson.* **1990,** 87, 628-32.

16. Palmer, A.G., III; Cavanaugh, J.; Wright, P.E.; Rance, M. Sensitivity Improvement in Proton-Detected Two-Dimensional Heteronuclear Correlation NMR Spectroscopy. *J. Magn. Reson.* **1991**, *93*, 151-70.

17. Kay, L.E.; Keifer, P.; Saarinen, T. Pure Absorption Gradient Enhanced Heteronuclear Single Quantum Correlation Spectroscopy with Improved Sensitivity. *J. Am. Chem. Soc.* **1992**, *114*, 10663-5.

18. Schleucher, J.; Schwendinger, M.; Sattler, M.; Schmidt, P.; Schedletzky, O.; Glazer, S.J.; Sorensen, O.W.; Griesinger, C. A General Enhancement Scheme in Heteronuclear Multidimensional NMR Employing Pulsed Field Gradients. *J. Biomol. NMR* **1994**, *4*, 301-6.

19. Hurd, R.E.; Boban, J.K. Gradient-Enhanced Proton-Detected Heteronuclear Multiple Quantum Coherence Spectroscopy. *J. Magn. Reson.* **1991,** *91*, 648-53.

20. Gibbs, S.J.; Johnson, C.S., Jr. A PFG NMR Experiment for Accurate Diffusion and Flow Studies in the Presence of Eddy Currents. *J. Magn. Reson.* **1991**, *93*, 395-402.

21. Silversteen, R.M.; Bassler, G.C.; Morrill, T.C. Spectrometric Identification of Organic Compounds, 5th ed. John Wiley and Sons, Inc.: New York, 1991; 171-77.

22. Aydin, R.; Loux, J-P.; Günther, H. Karplus Curve for $^{3}J(^{13}C, ^{1}H)$ in Hydrocarbons. *Agnew Chem. (Internat.)* **1982**, *21*, 499.

23. Kintz, P.; Villain, M.; Barguil, Y.; Charlot, J.Y.; Cirimele, V. Testing for Atropine and Scopolamine in Hair by LC-MS-MS after Datura Intoxia Abuse. *J. Anal. Tox.* **2006**, *30*, 454-7.

24. Oertel, R.; Richter, K.; Ebert, U.; Kirch, W. Determination of Scopolamine in Human Serum and Microdialysis Samples by Liquid Chromatography-Tandem Mass Spectrometry. *J. Chromatogr. B. Biomed. Sci. Appl.* **2001**, *750*, 121-8.

25. Beyer, J.; Peters, F.T.; Kramer, T.; Maurer, H.H. Detection and Validated Quantification of Toxic Alkaloids in Human Blood Plasma - Comparison of LC-APCI-MS with LC-ESI-MS/MS. *J. Mass. Spectrom.* In press.

26. Johns, S.R.; Lamberton, J.A. Magnetic Non-Equivalence of the Epoxide Ring (C-6 and C-7) Protons of Scopolamine. *J. Chem. Soc., Chem. Commun.* **1965**, 458-459.

27. Mandava, N.; Fodor, G. Configuration of the Ring Nitrogen in *N*-Oxides and the Conformation of Tropanes. Part XVIII. *Can. J. Chem.* **1968**, *46*, 2761-6.

28. Wenkert, E.; Bindra, J.S.; Chang, C-J.; Cochran, D.W.; Schell, F.M. Carbon-13 Nuclear Magnetic Resonance Spectroscopy of Naturally Occurring Substances. Alkaloids. *Acc. Chem. Res.* **1974**, *7*, 46-51.

29. Simeral, L.; Maciel, G.E. Carbon-13 Chemical Shifts of Some Cholinergic Neural Transmission Agents. *Org. Magn. Reson.* **1974**, *6*, 226-32.

30. Leete, E.; Kowanko, N.; Newmark, R.A. Use of Carbon-13 Nuclear Magnetic Resonance to Establish that the Biosynthesis of Tropic Acid Involves an Intramolecular Rearrangement of Phenylalanine. *J. Am. Chem. Soc.* **1975,** *97*, 6826-30.

31. Hanisch, P.; Jones, A.J.; Casey, A.F.; Coates, J.E. Carbon-13 Magnetic Resonance: Evidence for Non-Chair Conformations in Tropane Derivatives. *J. Chem. Soc., Perkin Trans.* **1976**, *2,* 1202-8.

32. Feeney, J.; Foster, R.; Piper, E.A. Nuclear Magnetic Resonance Study of the Conformations of Atropine and Scopolamine Cations in Aqueous Solution. *J. Chem. Soc., Perkin Trans.* **1977**, *2,* 2016-20.

33. Taha, A.M.; Rücher, G. ^{13}C-NMR Spectroscopy of Tropane Alkaloids. *J. Pharm. Sci.* **1978**, *67*, 775-9.

34. Mislow, K.; Siegel, J. Stereoisomerism and Local Chirality. *J. Am. Chem. Soc.* **1984**, *106*, 3319-28.

35. Chazin, W.J.; Colebrook, L.D. Use of Spin-Lattice Relaxation and Nuclear Overhauser Effect Data in Structure Analysis of Alkaloids. *J. Org. Chem.* **1986**, *51*, 1243-53.

36. Glaser, R.; Peng, Q-J.; Perlin, A.S. Stereochemistry of the *N*-Methyl Group in Salts of Tropane Alkaloids. *J. Org. Chem.* **1988**, *53*, 2172-80.

37. Glaser, R.; Charland, J-P.; Michel, A. Solid-State Stereochemistry of Anhydrous (-)-Scopolamine Hydrobromide. *J. Chem. Soc., Perkin Trans.* **1989**, *2,* 1875-89.

38. Sarazin, C.; Goethals, G. Séguin, J-P.; Barbotin, J-N. Spectral Reassignment and Structure Elucidation of Scopolamine Free Base through Two-Dimensional NMR Techniques. *Magn. Reson. Chem.* **1991,** *29*, 291-300.

39. Glaser, R. NMR and Molecular Mechanics Studies on the Solution-State Conformation of (-)-Scopolamine Free Base. *Magn. Reson. Chem.* **1993**, *31*, 335-9.

40. Michel, A.; Drouin, M.; Glaser, R. Solid-State Stereochemistry of (-)-Scopolamine Hydrobromide Sesquihydrate, a New Polymorph of the Cholinergic Drug. *J. Pharm. Sci.* **1994**, *83*, 508-13.

41. Naqui, A.A.; Mandal, S.; Verma, R.K. Determination of Atropine and Scopolamine by Proton Nuclear Magnetic Resonance Spectroscopy. *Phytochem. Anal.* **1998**, *9*, 168-70.

42. Glaser, R.; Shiftan, D.; Drouin, M. Conformational Psuedopolymorphism and Solid-State CPMAS NMR Studies for Determination of Solvent-Dependent Solution-State Conformational Preferences for (-)-Scopolamine Hydrobromide/Hydrochloride Salts. *J. Org. Chem.* **1999**, *64*, 9217-24.

43. Nakamura, M.; Yasumoto, T. Tetrodotoxin derivatives in Puffer Fish. *Toxicon.* **1985**, *23*, 271-6.

44. Yotsu-Yamashita, M.; Schimmele, B.; Yasumoto, T. Isolation and Structural Assignment of 5-Deoxytetrodotoxin from the Puffer Fish Fufu Poecilonotus. *Biosci. Biotechnol. Biochem.* **1999**, *63*, 961-3.

45. Kondo, T.; Kurihara, S.; Yoshikawa, T.; Mizukami, H. Effect of N- and C-Terminal Deletions on the RNA *N*-Glycosidase Activity and the Antigenicity of Karasurin-A, a Ribosome Inactivating Protein from *Trichosanthes kirilowii* var. *japonica*. *Biotechnol. Lett.* **2004,** *26*, 1873-8.

46. He, W.J.; Liu, W.Y. Both N- and C-Terminal Regions are Essential for Cinnamomin A-Chain to Deadenylate Ribosomal RNA and Supercoiled Double Stranded DNA. *Biochem. J.* **2004**, *377*, 17-23.

47. Herrero, S.; Gonzalez-Cabrera, J.; Ferre, J.; Bakker, P.L.; de Maagd, R.A. Mutations in the *Bacillus thuringiensis* Cry1Catoxin Demonstrate the role of Domains II and III in Specificity towards Spodoptera Exigua Larvae. *Biochem. J.* **2004,** *384*, 507-13.

48. Dai, Q.; Castellino, F.J.; Prorok, M. A Single Amino Acid Replacement Results in the Ca^{2+}-Induced Self Assembly of a Helical Conantokin-Based Peptide. *Biochemistry* **2004**, *43*, 13225-32.

49. Clark, R.J.; Fischer, H.; Dempster, L.; Daly, N.L.; Rosengren, K.J.; Nevin, S.T.; Maunier, F.A.; Adams, D.J.; Craik, D.J. Engineering Stable Peptide Toxins by Means of Backbone Cyclization: Stabilization of the Alpha-Conotoxin MII. *Proc. Natl. Acad. Sci. USA* **2005**, *102*, 13767-72.

50. Morinaga, N.; Yahiro, K.; Matsurra, G.; Watanabe, M.; Nomura, F.; Moss, J.; Noda, M. Two Distinct Cytotoxic Acitvities of Subtilase Cytotoxin Produced by Shiga-Toxingenic *Escherichia coli*. *Infect. Immun.* **2007**, *75*, 488-96.